applied sciences

MDPI

Article

Shear Strength of Trapezoidal Corrugated Steel Webs for Horizontally Curved Girder Bridges

Sumei Liu [1,2], Hanshan Ding [1,*], Luc Taerwe [2,3] and Wouter De Corte [2]

1 School of Civil Engineering, Southeast University, Nanjing 210096, China; lsmf@seu.edu.cn
2 Department of Structural Engineering, Faculty of Engineering and Architecture, Ghent University, 9000 Ghent, Belgium; Luc.Taerwe@UGent.be (L.T.); Wouter.DeCorte@UGent.be (W.D.C.)
3 College of Civil Engineering, Tongji University, Shanghai 200092, China
* Correspondence: hsding@seu.edu.cn

Received: 11 April 2019; Accepted: 7 May 2019; Published: 12 May 2019

Abstract: Curved composite girder bridges with corrugated steel webs (CSWs) have already been constructed around the world. However, limited work has been done on their shear behavior. In this paper, the corrugated steel web (CSW) in horizontally curved girders (HCGs) is treated as an orthotropic cylindrical shallow shell, and the analytical formula for the elastic global shear buckling stress is deduced by the Galerkin method. Calculation tables for the global shear buckling coefficient for a four-edge simple support, for a four-edge fixed support, and for the two edges constrained by flanges fixed and the other two edges simply supported are given. Then, a parametric study based on a linear buckling analysis is performed to analyze the effect of the curvature radius and girder span on the shear buckling stress. Analytical and numerical results show that the difference of shear buckling stress of CSWs between curved girders and straight girders is small, so the shear design formulas for straight girders can be applied for curved girders. Finally, a series of tests were performed on three curved box girders with CSWs. Similar to CSWs in straight girders, the shear strain distributions of CSWs in HCGs are almost uniform along the direction of the web height and the principal strain direction angles are close to 45°. For the three specimens, CSWs carry about 76% of the shear force. In the destructive test, shear buckling after yielding occurred in all specimens which is in good agreement with the theoretical prediction, which means that the analytical formulas provide good predictions for the shear buckling stress of CSWs in HCGs and can be recommended for design purposes.

Keywords: horizontally curved girder; corrugated steel webs; shear buckling stress; Galerkin method; finite element analysis; experimental work

1. Introduction

The steel-concrete composite girder with CSWs is known as a new type of bridge structure to overcome the weight problem of common concrete box girders. Compared with concrete webs, CSWs have low longitudinal stiffness due to the accordion effect, so CSWs mainly carry the shear force and barely carry axial force [1]. Because of this characteristic, CSWs fail due to shear buckling or yielding. Therefore, the shear buckling stability of CSWs is one of the most important considerations in the design of this kind of composite girder bridges.

Curved composite girder bridges with CSWs (see Figure 1) have already been constructed around the world, for example, the Meaux viaduct in France, the Altwipfergrund viaduct in Germany, the Nakano viaduct in Japan, the Yuwotou bridge and No. 3 East River bridge in China, etc. However, so far, limited research has been conducted on the shear behavior of CSWs of HCGs. In practice, the shear buckling calculation of CSWs for HCGs usually adopts the corresponding formula of straight

girders which have been relatively well studied. It is widely accepted that for straight girder bridges, local shear buckling is the dominant failure mode in coarse corrugations, whereas global shear buckling becomes the dominant failure mode in dense corrugations and interactive shear buckling mode becomes dominant when the density is in between of the two above scenarios [2]. It is straightforward to understand that the shear buckling failure modes of CSWs in HCGs also consist of local shear buckling, global shear buckling, and interactive shear buckling.

(**a**) (**b**)

Figure 1. Curved composite girder bridges with corrugated steel webs (CSWs): (**a**) Altwipfergrund Viaduct; (**b**) Yuwotou Bridge. CSW: corrugated steel web.

The local shear buckling of CSWs for straight girders is solved by analyzing a single flat panel constrained by adjacent panels and girder flanges under shear force. For this, the formula for the shear buckling stress of isotropic rectangular plates [3] can be applied. Because the single flat panel of CSWs in HCGs is under the same constraint conditions as in straight girders, the formula can also be applied to HCGs. Aggarwal et al. [4] numerically studied the local shear buckling of CSWs and found that the boundary conditions at the top and bottom edges were close to fixed, while the boundary conditions at the fold line between the flat and inclined panels lie between simply supported and fixed.

The global shear buckling of CSWs for straight girder bridges is analyzed by assuming the whole web as an orthotropic rectangular plate constrained by concrete flanges and diaphragms, and has been studied by various researchers. Bergman and Reissner [5] derived the formula for calculating shear buckling loads by treating the corrugated plates as plates having different flexural rigidities in two perpendicular directions. Hlavacek [6] investigated the shear buckling behavior of stiffened plates reinforced by separate equally spaced stiffeners which were symmetrically arranged on two sides of the plates, and extended the deduced results to corrugated plates. Easley and McFarland [7] investigated the global shear buckling behavior of corrugated metal diaphragms also by treating them as orthotropic plates and developed the formulas for the shear buckling load by the Ritz and the Energy method. Easley [8] made a comparative analysis of the Bergmann-Reissner formula [5], the Hlavacek formula [6] and the Easley-McFarland formula [7], and proposed a more comprehensive and applicable global shear buckling formula of corrugated plates. Corrugated plates were originally applied in aircrafts and were gradually extended to civil engineering. The formula $\tau_g^e = k_g \frac{(D_x)^{1/4}(D_y)^{3/4}}{th^2}$ was accepted to calculate the global shear buckling stress of CSWs for straight girders, where k_g is the global shear buckling coefficient depending on the edge conditions. Although a global shear buckling formula of CSWs has been proposed, researchers hold different views on the global shear buckling coefficient k_g. Easley [8] proposed $36 \le k_g \le 68.4$, 36 for a four-edge simple support and 68.4 for a four-edge fixed support, while Peterson [9] and Bergfelt et al. [10] suggested 32.4 for a four-edge simple support and 60.4 for a four-edge fixed support, and El Metwally and Loov [11] suggested 50 for composite girders with CSWs. The Guide to Stability Design Criteria for Metal Structures adopted 31.6 for a four-edge simple support and 59.2 for a four-edge fixed support [12]. Machimdamrong et al. [13] presented the transition curves of the elastic global shear buckling capacity from the case of a four-edge simple support to the case of a four-edge fixed support using the Rayleigh-Ritz method, but provides only the curves for the plate dimensions ($l \times h$) of 1 m × 1 m and 2 m × 1 m.

Finally, the interactive shear buckling formula for CSWs is determined by local shear buckling, global shear buckling and the yield stress of the plate material [14], but the way these parameters are to be combined is still the subject of debate. Important work has been done by Bergfelt et al. [10], El Metwally [15], Abbas et al. [16], Shiratani et al. [17], Sayed-Ahmed [18] and Yi et al. [14], etc., and various interactive shear buckling formulas of CSWs were proposed.

For practical applications, Elgaaly et al. [19] recommended that the capacity of CSWs was controlled by the smaller value of local and global buckling, and a semiempirical formula for the inelastic buckling stress when the elastic buckling stress is larger than 80% of the yield stress was proposed. Driver et al. [20] proposed a lower bound equation by combining local and global shear buckling equations of CSWs. Moon et al. [21] proposed a shear buckling parameter formula for trapezoidal CSWs with no need to calculate either local, global or interactive shear buckling parameters. Eldib [2] proposed a shear buckling parameter formula for curved CSWs. Nie et al. [22] carried out eight H-shape steel girders with CSWs and proposed a formula for the shear strength prediction of trapezoidal CSWs. Hassanein et al. investigated the shear behavior of linearly tapered bridge girders with CSWs [23], and high-strength steel corrugated web girders [24]. Leblouba and Barakat [25] experimentally and numerically studied the shear stress distribution in trapezoidal CSWs.

Basher et al. [26] studied the ultimate shear behavior of HCGs with trapezoidal CSWs and proposed an approximate method to calculate the shear strength of these girders. The ultimate shear strength of curved girders uses the equation of straight girders introducing a modification factor to account for the curvature of curved girders. Wang et al. [27] theoretically and numerically studied the elastic global shear buckling of HCGs with CSWs and proposed a global shear buckling stress formula for a four-edge simple support. From the studies mentioned above, it is clear that a lot of work has been done related to the shear behavior of straight girders with CSWs, but limited work to HCGs. The curvature of HCGs may indeed have an influence on the buckling of CSWs. Therefore, a comprehensive study is necessary to understand whether the shear buckling formulas for CSWs for straight girders are appropriate for HCGs, and if so, to which extent.

In this study, the CSW in HCGs is treated as an orthotropic cylindrical shallow shell constrained by the concrete flanges and diaphragms. First, the analytical formula for the elastic global shear buckling stress for three boundary conditions is deduced by the Galerkin method. Then, a parametric study based on a linear buckling analysis is performed to analyze the effect of the curvature radius and girder span on the shear buckling stress. Finally, a series of tests performed on three box girders with CSWs is discussed.

2. Elastic Global and Local Shear Buckling Stress of CSWs

2.1. Physical Equivalent Parameters of CSWs

For trapezoidal CSWs that are commonly used in actual girder bridges, when treated as an orthotropic plate or shell, the equivalent poisson's ratios v_x, v_y [28], the equivalent elastic moduli E_x, E_y, the equivalent shear modulus G_{xy} [29], the equivalent flexural stiffnesses D_x, D_y and the torsional stiffness D_{xy} per unit length of a CSW [7] can be expressed as Equations (1)–(8).

$$v_x = v\frac{E_x}{E} \tag{1}$$

$$v_y = v \tag{2}$$

$$E_x = \frac{t^2(a+b)}{d^2(3a+c)}E \tag{3}$$

$$E_y = \frac{s}{q}E \tag{4}$$

$$G_{xy} = \frac{q}{s}G \tag{5}$$

$$D_x = \frac{q}{s}\frac{Et^3}{12} \tag{6}$$

$$D_y = \frac{E(3a+c)td^2}{6q} \tag{7}$$

$$D_{xy} = \frac{s}{q}\frac{Et^3}{6(1+\nu)} \tag{8}$$

where v, E, G are the poisson's ratio, the elastic modulus and the shear modulus of original steel plate respectively, and t is the web thickness. As shown in Figure 1b, a is the flat panel width; b is the horizontal projection width of the inclined panel; c is the inclined panel width; d is the corrugation depth; θ is the corrugation angle; q is the horizontal projection length of one periodic corrugation; s is the total folded panel length of one periodic corrugation.

2.2. Elastic Global Shear Buckling Stress of CSWs

2.2.1. Critical Buckling Stress under Pure Shear

According to the theory of thin plates and shells, if the ratio of a shell's height to its short side is less than 0.2, the shell can be analyzed as a shallow shell. For HCGs with vertical CSWs, webs always meet this condition and can be treated as orthotropic cylindrical shallow shells (Figure 2) for the global shear buckling analysis.

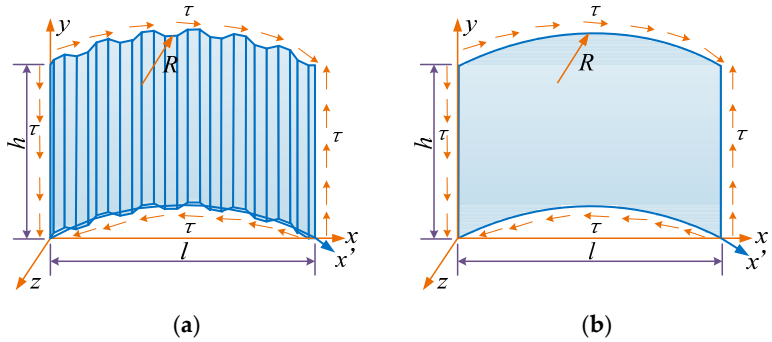

Figure 2. Corrugated steel web and its equivalent orthotropic cylindrical shallow shell: (**a**) Corrugated steel web; (**b**) Equivalent orthotropic cylindrical shallow shell.

According to the stability theory of plates and shells, the equilibrium equation and the deformation compatibility equation of an orthotropic cylindrical shallow shell shown in Figure 2 under pure shear force can be expressed respectively as Equations (9) and (10) [30]. In the following equations, the part that appears in bold type shows the difference between a plate and a shell.

$$\frac{1}{t}\left(D_x\frac{\partial^4}{\partial x^4} + D_{xy}\frac{\partial^4}{\partial x^2\partial y^2} + D_y\frac{\partial^4}{\partial y^4}\right)w + \frac{\mathbf{1}}{\boldsymbol{R}}\frac{\boldsymbol{\partial^2\Phi}}{\boldsymbol{\partial y^2}} = 2\tau\frac{\partial^2 w}{\partial x\partial y} \tag{9}$$

$$\left[\frac{1}{E_y}\frac{\partial^4}{\partial x^4} + \left(\frac{1}{G_{xy}} - 2\frac{\nu_y}{E_y}\right)\frac{\partial^4}{\partial x^2\partial y^2} + \frac{1}{E_x}\frac{\partial^4}{\partial y^4}\right]\Phi - \frac{\mathbf{1}}{\boldsymbol{R}}\frac{\boldsymbol{\partial^2 w}}{\boldsymbol{\partial y^2}} = 0 \tag{10}$$

where $\boldsymbol{\Phi}$ is the stress function, w is the out of plane deflection of the shell, τ is the shear stress, R is the curvature radius of the HCG.

Substituting Equation (10) into Equation (9), Equation (9) can be expressed as Equation (11).

$$\frac{1}{t}\left(D_x\frac{\partial^4}{\partial x^4} + D_{xy}\frac{\partial^4}{\partial x^2\partial y^2} + D_y\frac{\partial^4}{\partial y^4}\right)w + \frac{\mathbf{1}}{\boldsymbol{R^2}}\left[\frac{\mathbf{1}}{\boldsymbol{E_y}}\frac{\boldsymbol{\partial^4}}{\boldsymbol{\partial x^4}} + \left(\frac{\mathbf{1}}{\boldsymbol{G_{xy}}} - \mathbf{2}\frac{\boldsymbol{\nu_y}}{\boldsymbol{E_y}}\right)\frac{\boldsymbol{\partial^4}}{\boldsymbol{\partial x^2\partial y^2}} + \frac{\mathbf{1}}{\boldsymbol{E_x}}\frac{\boldsymbol{\partial^4}}{\boldsymbol{\partial y^4}}\right]^{\boldsymbol{-1}}\frac{\boldsymbol{\partial^4 w}}{\boldsymbol{\partial y^4}} = 2\tau\frac{\partial^2 w}{\partial x\partial y} \tag{11}$$

It can be assumed that the boundary conditions of CSWs satisfy a four-edge simple support, a four-edge fixed support, or the two edges constrained by flanges fixed and the other two edges simply supported (the edges $x = 0$ and $x = l$ are simply supported, the edges $y = 0$ and $y = h$ are fixed supported). The functions of deflection can be expressed respectively as Equations (12)–(14).

For a four-edge simple support [3]:

$$w = \sum_{m=1}^{\infty}\sum_{n=1}^{\infty} A_{mn} \sin\frac{m\pi x}{l} \sin\frac{n\pi y}{h} \tag{12}$$

For a four-edge fixed support [31]:

$$w = \sum_{m=1}^{\infty}\sum_{n=1}^{\infty} A_{mn}\left[\frac{1}{m}\sin\frac{m\pi x}{l} - \frac{1}{m+2}\sin\frac{(m+2)\pi x}{l}\right]\left[\frac{1}{n}\sin\frac{n\pi y}{h} - \frac{1}{n+2}\sin\frac{(n+2)\pi y}{h}\right] \tag{13}$$

For the edges $x = 0$ and $x = l$ simply supported, and the edges $y = 0$ and $y = h$ fixed:

$$w = \sum_{m=1}^{\infty}\sum_{n=1}^{\infty} A_{mn} \sin\frac{m\pi x}{l}\left[\frac{1}{n}\sin\frac{n\pi y}{h} - \frac{1}{n+2}\sin\frac{(n+2)\pi y}{h}\right] \tag{14}$$

where h is the web height equal to the clear distance between the top and bottom concrete flanges, l is the web length equal to the linear distance between the two adjacent diaphragm plates.

By substituting Equations (12)–(14) into Equation (11), defining $\alpha = \frac{D_x}{D_y} = \frac{E_x}{E_y}$, $\beta = \frac{D_{xy}}{D_y}$, $\gamma = \frac{G_{xy}}{E_y - 2\nu_y G_{xy}}$, $\lambda = l/h$, considering $\frac{E_y}{D_y} = \frac{6s}{td^2(3a+c)}$, and according to the Galerkin method, Equation (11) can be simplified as Equations (15)–(17) respectively.

For the four-edge simple support:

$$\begin{aligned}&\frac{D_y}{4th^2}\left[\frac{\pi^4}{\lambda^3}\left(\alpha m^4 + \beta\lambda^2 m^2 n^2 + \lambda^4 n^4\right) + \boldsymbol{\alpha\gamma\lambda^5 n^4}\left(\boldsymbol{\alpha\gamma m^4 + \alpha\lambda^2 m^2 n^2 + \gamma\lambda^4 n^4}\right)^{-1}\frac{h^4}{R^2 d^2}\frac{6s}{(3a+c)}\right]A_{mn}\\ &-8\tau\sum_{i}^{\infty}\sum_{j}^{\infty} A_{ij}\frac{mnij}{(m^2-i^2)(n^2-j^2)} = 0(m \pm i = \text{odd}, n \pm j = \text{odd})\end{aligned} \tag{15}$$

For the four-edge fixed support:

$$\begin{aligned}&\frac{D_y}{th^2}\frac{\pi^4}{4\lambda^3}\left\{\begin{array}{l}A_{mn}\left\{\alpha\left[m^2+(m+2)^2\right]\left[n^{-2}+(n+2)^{-2}\right] + 4\beta\lambda^2 + \lambda^4\left[m^{-2}+(m+2)^{-2}\right]\left[n^2+(n+2)^2\right]\right\}\\ -A_{m,n+2}\left\{\alpha\left[m^2+(m+2)^2\right](n+2)^{-2} + 2\beta\lambda^2 + \lambda^4\left[m^{-2}+(m+2)^{-2}\right](n+2)^2\right\}\\ -A_{m,n-2}\left\{\alpha\left[m^2+(m+2)^2\right]n^{-2} + 2\beta\lambda^2 + \lambda^4\left[m^{-2}+(m+2)^{-2}\right]n^2\right\}\\ -A_{m+2,n}\left\{\alpha(m+2)^2\left[n^{-2}+(n+2)^{-2}\right] + 2\beta\lambda^2 + \lambda^4(m+2)^{-2}\left[n^2+(n+2)^2\right]\right\}\\ +A_{m+2,n+2}\left[\alpha(m+2)^2(n+2)^{-2} + \beta\lambda^2 + \lambda^4(m+2)^{-2}(n+2)^2\right]\\ +A_{m+2,n-2}\left[\alpha(m+2)^2 n^{-2} + \beta\lambda^2 + \lambda^4(m+2)^{-2}n^2\right]\\ -A_{m-2,n}\left\{\alpha m^2\left[n^{-2}+(n+2)^{-2}\right] + 2\beta\lambda^2 + \lambda^4 m^{-2}\left[n^2+(n+2)^2\right]\right\}\\ +A_{m-2,n+2}\left[\alpha m^2(n+2)^{-2} + \beta\lambda^2 + \lambda^4 m^{-2}(n+2)^2\right]\\ +A_{m-2,n-2}\left[\alpha m^2 n^{-2} + \beta\lambda^2 + \lambda^4 m^{-2}n^2\right]\end{array}\right\}\\ &+\frac{D_y}{th^2}\frac{h^4}{R^2d^2}\frac{6s}{(3a+c)}\frac{\alpha\gamma\lambda^5}{4}\left\{\begin{array}{l}\boldsymbol{A_{mn}}\left\{\begin{array}{l}\left(\boldsymbol{\alpha\gamma m^4 + \alpha\lambda^2 m^2 n^2 + \gamma\lambda^4 n^4}\right)^{-1}\boldsymbol{m^{-2}n^2}\\ +\left[\boldsymbol{\alpha\gamma m^4 + \alpha\lambda^2 m^2(n+2)^2 + \gamma\lambda^4(n+2)^4}\right]^{-1}\boldsymbol{m^{-2}(n+2)^2}\\ +\left[\boldsymbol{\alpha\gamma(m+2)^4 + \alpha\lambda^2(m+2)^2 n^2 + \gamma\lambda^4 n^4}\right]^{-1}\boldsymbol{(m+2)^{-2}n^2}\\ +\left[\boldsymbol{\alpha\gamma(m+2)^4 + \alpha\lambda^2(m+2)^2(n+2)^2 + \gamma\lambda^4(n+2)^4}\right]^{-1}\boldsymbol{(m+2)^{-2}(n+2)^2}\end{array}\right\}\\ -\boldsymbol{A_{m,n+2}}\left\{\begin{array}{l}\left[\boldsymbol{\alpha\gamma m^4 + \alpha\lambda^2 m^2(n+2)^2 + \gamma\lambda^4(n+2)^4}\right]^{-1}\boldsymbol{m^{-2}(n+2)^2}\\ +\left[\boldsymbol{\alpha\gamma(m+2)^4 + \alpha\lambda^2(m+2)^2(n+2)^2 + \gamma\lambda^4(n+2)^4}\right]^{-1}\boldsymbol{(m+2)^{-2}(n+2)^2}\end{array}\right\}\\ -\boldsymbol{A_{m,n-2}}\left\{\begin{array}{l}\left(\boldsymbol{\alpha\gamma m^4 + \alpha\lambda^2 m^2 n^2 + \gamma\lambda^4 n^4}\right)^{-1}\boldsymbol{m^{-2}n^2}\\ +\left[\boldsymbol{\alpha\gamma(m+2)^4 + \alpha\lambda^2(m+2)^2 n^2 + \gamma\lambda^4 n^4}\right]^{-1}\boldsymbol{(m+2)^{-2}n^2}\end{array}\right\}\\ -\boldsymbol{A_{m+2,n}}\left\{\begin{array}{l}\left[\boldsymbol{\alpha\gamma(m+2)^4 + \alpha\lambda^2(m+2)^2 n^2 + \gamma\lambda^4 n^4}\right]^{-1}\boldsymbol{(m+2)^{-2}n^2}\\ +\left[\boldsymbol{\alpha\gamma(m+2)^4 + \alpha\lambda^2(m+2)^2(n+2)^2 + \gamma\lambda^4(n+2)^4}\right]^{-1}\boldsymbol{(m+2)^{-2}(n+2)^2}\end{array}\right\}\\ +\boldsymbol{A_{m+2,n+2}}\left[\boldsymbol{\alpha\gamma(m+2)^4 + \alpha\lambda^2(m+2)^2(n+2)^2 + \gamma\lambda^4(n+2)^4}\right]^{-1}\boldsymbol{(m+2)^{-2}(n+2)^2}\\ +\boldsymbol{A_{m+2,n-2}}\left[\boldsymbol{\alpha\gamma(m+2)^4 + \alpha\lambda^2(m+2)^2 n^2 + \gamma\lambda^4 n^4}\right]^{-1}\boldsymbol{(m+2)^{-2}n^2}\\ -\boldsymbol{A_{m-2,n}}\left\{\begin{array}{l}\left(\boldsymbol{\alpha\gamma m^4 + \alpha\lambda^2 m^2 n^2 + \gamma\lambda^4 n^4}\right)^{-1}\boldsymbol{m^{-2}n^2}\\ +\left[\boldsymbol{\alpha\gamma m^4 + \alpha\lambda^2 m^2(n+2)^2 + \gamma\lambda^4(n+2)^4}\right]^{-1}\boldsymbol{m^{-2}(n+2)^2}\end{array}\right\}\\ +\boldsymbol{A_{m-2,n+2}}\left[\boldsymbol{\alpha\gamma m^4 + \alpha\lambda^2 m^2(n+2)^2 + \gamma\lambda^4(n+2)^4}\right]^{-1}\boldsymbol{m^{-2}(n+2)^2}\\ +\boldsymbol{A_{m-2,n-2}}\left(\boldsymbol{\alpha\gamma m^4 + \alpha\lambda^2 m^2 n^2 + \gamma\lambda^4 n^4}\right)^{-1}\boldsymbol{m^{-2}n^2}\end{array}\right\}\\ &-8\tau\sum_{i=1}^{\infty}\sum_{j=1}^{\infty} A_{ij}\left\{\begin{array}{l}\left[\frac{1}{m^2-i^2} - \frac{1}{(m+2)^2-i^2} - \frac{1}{m^2-(i+2)^2} + \frac{1}{(m+2)^2-(i+2)^2}\right]\\ \times\left[\frac{1}{n^2-j^2} - \frac{1}{(n+2)^2-j^2} - \frac{1}{n^2-(j+2)^2} + \frac{1}{(n+2)^2-(j+2)^2}\right]\end{array}\right\} = 0\end{aligned} \tag{16}$$

For the edges $x = 0$ and $x = l$ simply supported, and the edges $y = 0$ and $y = h$ fixed:

$$\begin{aligned}
&\frac{D_y}{th^2}\frac{\pi^4}{4\lambda^3}\left\{\begin{array}{l} A_{mn}\left\{\alpha m^4\left[n^{-2}+(n+2)^{-2}\right]+2\beta\lambda^2m^2+\lambda^4\left[n^2+(n+2)^2\right]\right\} \\ -A_{m,n+2}\left[\alpha m^4(n+2)^{-2}+\beta\lambda^2m^2+\lambda^4(n+2)^2\right]-A_{m,n-2}\left[\alpha m^4n^{-2}+\beta\lambda^2m^2+\lambda^4n^2\right]\end{array}\right\} \\
&+\frac{D_y}{th^2}\frac{h^4}{R^2d^2}\frac{6s}{(3a+c)}\frac{\alpha\gamma\lambda^5}{4}\left\{\begin{array}{l} A_{mn}\left\{\begin{array}{l}\left(\alpha\gamma m^4+\alpha\lambda^2m^2n^2+\gamma\lambda^4n^4\right)^{-1}n^2 \\ +\left[\alpha\gamma m^4+\alpha\lambda^2m^2(n+2)^2+\gamma\lambda^4(n+2)^4\right]^{-1}(n+2)^2\end{array}\right\} \\ -A_{m,n+2}\left[\alpha\gamma m^4+\alpha\lambda^2m^2(n+2)^2+\gamma\lambda^4(n+2)^4\right]^{-1}(n+2)^2 \\ -A_{m,n-2}\left(\alpha\gamma m^4+\alpha\lambda^2m^2n^2+\gamma\lambda^4n^4\right)^{-1}n^2\end{array}\right\} \\
&-8\tau\sum_{i=1}^{\infty}\sum_{j=1}^{\infty}A_{ij}\frac{mi}{m^2-i^2}\left[\frac{1}{n^2-j^2}-\frac{1}{(n+2)^2-j^2}-\frac{1}{n^2-(j+2)^2}+\frac{1}{(n+2)^2-(j+2)^2}\right]=0
\end{aligned} \tag{17}$$

By assigning values to m and n in Equations (15)–(17), a series of linear algebraic equations with A_{ij} as unknowns can be obtained. Then the critical shear buckling stress can be derived by assuming the coefficient determinant of the linear algebraic equations equals zero. (i.e., a linear bifurcation analysis).

According to Equations (15)–(17), the elastic global shear buckling stress of CSWs can be expressed as Equation (18):

$$\tau_g^e = k_g\frac{D_y}{h^2t} \tag{18}$$

where k_g is the elastic global shear buckling coefficient of CSWs in HCGs. The detailed solution process of the coefficient $k_{g,s}$ for a four-edge simple support, $k_{g,f}$ for a four-edge fixed support, $k_{g,fs}$ for the edges $x = 0$ and $x = l$ simply supported, and the edges $y = 0$ and $y = h$ fixed is given below.

2.2.2. Calculation of Coefficient k_g

According to Equations (15)–(18), the global shear buckling coefficient of CSWs in HCGs k_g is associated with the length to height ratio λ (l/h), the rigidity ratios $\alpha(D_x/D_y)$ and $\beta(D_{xy}/D_y)$, the modulus ratio $\gamma(G_{xy}/(E_y - 2\nu_yG_{xy}))$, the expression $h^2/(Rd)$ and $6s/(3a + c)$.

1. Value ranges of α, β, γ, $h^2/(Rd)$ and $6s/(3a + c)$ for common HCG bridges with CSWs

For trapezoidal CSWs that are commonly used in girder bridges, the rigidity ratios α and β have the relationship: $\beta/\alpha = 2s^2/[(1 + \nu)q^2]$. A statistical analysis of available bridges with CSWs (as shown in Table 1) shows that the rigidity ratio α varies from 0.0006 to 0.0069, γ varies from 0.38 to 0.44, $6s/(3a + c)$ is about 6, and β is about $(1.67\sim2.0)\alpha$. The following parametric study considers α ranging from 0.0005 to 0.0070, γ ranging from 0.38 to 0.44, $6s/(3a + c)$ equal to 6 and β equal to 1.6α, 1.8α, 2.0α respectively.

Table 1. The geometry of CSWs in available bridges.

Bridges	a	c	d	t_{min}	t_{max}	$\frac{6s}{3a+c}$	Corresponding to t_{min}			Corresponding to t_{max}			γ
	mm	mm	mm	mm	mm		α	β	β/α	α	β	β/α	
Cognac	353	353	150	8	8	6.00	0.0013	0.0022	1.69	0.0013	0.0022	1.69	0.4406
Maupre	284	284	150	8	8	6.00	0.0012	0.0022	1.83	0.0012	0.0022	1.83	0.4093
Dole	430	430	220	8	12	6.00	0.0006	0.0010	1.67	0.0013	0.0023	1.77	0.4159
Shinkai	250	250	150	9	9	6.00	0.0015	0.0028	1.87	0.0015	0.0028	1.87	0.3832
Miyukibashi	300	300	150	8	12	6.00	0.0012	0.0022	1.83	0.0028	0.0049	1.75	0.4193
Katsutegawa	430	430	220	9	12	6.00	0.0007	0.0013	1.86	0.0013	0.0023	1.77	0.4159
Hontani	330	336	200	9	14	6.03	0.0008	0.0016	2.00	0.0020	0.0038	1.90	0.3841
Koinumarukawa	430	430	220	9	16	6.00	0.0007	0.0013	1.86	0.0023	0.0041	1.78	0.4159
Shimoda	430	430	220	12	16	6.00	0.0013	0.0023	1.77	0.0023	0.0041	1.78	0.4159
Nakano Viaduct	330	336	200	9	19	6.03	0.0008	0.0016	2.00	0.0037	0.0069	1.86	0.3841
Kurobekawa Railway	400	400	200	12	25	6.00	0.0016	0.0028	1.75	0.0069	0.0120	1.74	0.4240
Altwipfergrund	360	360	220	10	22	6.00	0.0008	0.0016	2.00	0.0041	0.0077	1.88	0.3832
Juancheng-Huanghe	430	421	200	10	18	5.97	0.0011	0.0019	1.73	0.0036	0.0062	1.72	0.4270
Henan-Pohe	250	250	150	8	8	6.00	0.0012	0.0022	1.83	0.0012	0.0022	1.83	0.3832
Wei River	330	336	200	8	12	6.03	0.0007	0.0012	1.71	0.0015	0.0028	1.87	0.3841
Nanjing-Chuhe	430	430	220	10	18	6.00	0.0009	0.0016	1.78	0.0029	0.0051	1.76	0.4159

Note: t_{max} and t_{min} are the maximum and minimum thicknesses of CSWs respectively when an available bridge has more than one thickness value.

Table 1 shows that the corrugation depth d varies from 0.15 m to 0.22 m. The upper limit of H/d does not exceed 133 considering the girder height H generally is not more than 20 m. For common HCG bridges, the girder height to length ratio H/L generally ranges from 1/11 to 1/30, and the central angle L/R is generally no more than $\pi/2$. So, the upper limit of H/R of HCG bridges does not exceed 0.143, where L is the girder span. Thus, the upper limit of $H^2/(Rd)$ of HCG bridges does not exceed 20. Because the CSW height h is smaller than the girder height H, the upper limit of $h^2/(Rd)$ does not exceed 20. In order to expand the scope of application of the formulas, the following parametric study considers $h^2/(Rd)$ ranging from 0 to 30.

2. Influence of α and β/α on the global shear buckling coefficient k_g

Theoretically, the more numbers used in the trigonometric series (as shown in Equations (12)–(14)), the more precise the solution is. If m and n increase toward infinity, exact results of shear buckling stress of CSWs can be obtained. However, the calculation effort increases with the increasing numbers m and n in the trigonometric series. In the case of the CSW with a length to height ratio l/h less than 5, the deviation between the results with $m = 30$, $n = 30$ and the results with $m = 25$, $n = 25$ is less than 1%. In what follows, $m = 30$ and $n = 30$ are adopted.

Table 2 shows the values of k_g calculated for various values of D_x/D_y and l/h, and for $\beta = 1.6\alpha$, $\beta = 1.8\alpha$ and $\beta = 2.0\alpha$ respectively when $h^2/(Rd) = 5$ and $\gamma = 0.4$ for a four-edge simple support. The results for $\beta = 1.6\alpha$ and $\beta = 2.0\alpha$, compared to for $\beta = 1.8\alpha$, deviate less than 0.6%. The results show that the parameter β/α has little effect on the coefficient k_g for common bridges with CSWs. From an engineering application point of view, the deviations can be ignored. In addition, the conclusion remains unchanged when changing the values of $h^2/(Rd)$, γ, and the boundary conditions. As a result, $\beta = 1.8\alpha$ is used further in this paper.

Table 2. The effect of β/α on the global shear buckling coefficient $k_{g,s}$ when $h^2/(Rd) = 5$ and $\gamma = 0.4$ for the four-edge simple support.

D_x/D_y		l/h				
		1	**2**	**3**	**4**	**5**
0.0005	$\beta = 1.6\alpha$	5.0169	4.9471	4.9335	4.9292	4.9252
	$\beta = 1.8\alpha$	5.0245	4.9547	4.9410	4.9367	4.9327
	$\beta = 2.0\alpha$	5.0321	4.9623	4.9486	4.9442	4.9402
0.0015	$\beta = 1.6\alpha$	6.7307	6.5947	6.5643	6.5525	6.5470
	$\beta = 1.8\alpha$	6.7489	6.6121	6.5816	6.5697	6.5642
	$\beta = 2.0\alpha$	6.7671	6.6295	6.5989	6.5868	6.5813
0.0025	$\beta = 1.6\alpha$	7.7454	7.5645	7.5126	7.4963	7.4888
	$\beta = 1.8\alpha$	7.7714	7.5901	7.5379	7.5214	7.5139
	$\beta = 2.0\alpha$	7.7973	7.6151	7.5631	7.5465	7.5390
0.0035	$\beta = 1.6\alpha$	8.5136	8.2755	8.2214	8.2008	8.1909
	$\beta = 1.8\alpha$	8.5485	8.3084	8.2539	8.2332	8.2232
	$\beta = 2.0\alpha$	8.5834	8.3413	8.2865	8.2656	8.2555
0.0050	$\beta = 1.6\alpha$	9.5393	9.1230	9.0567	9.0301	9.0159
	$\beta = 1.8\alpha$	9.5816	9.1656	9.0993	9.0721	9.0580
	$\beta = 2.0\alpha$	9.6239	9.2081	9.1418	9.1141	9.1001
0.0070	$\beta = 1.6\alpha$	10.4099	10.0444	9.9332	9.8997	9.8847
	$\beta = 1.8\alpha$	10.4672	10.1004	9.9878	9.9537	9.9386
	$\beta = 2.0\alpha$	10.5245	10.1557	10.0424	10.0077	9.9924

Figure 3 shows the effect of the rigidity ratio D_x/D_y and the length to height ratio l/h on the global shear buckling coefficient $k_{g,s}$ for a four-edge simple support. As we can see from Figure 3, the global shear buckling coefficient $k_{g,s}$ increases with the increase of the rigidity ratio D_x/D_y and decreases with the increase of the length to height ratio l/h but only very little. When l/h is larger than

2, which is common for bridges, the change of $k_{g,s}$ is minimal and the values of $k_{g,s}$ show a converging trend. The conclusion remains unchanged when changing the values of $h^2/(Rd)$, γ, and the boundary conditions. Because the values of k_g show a converging trend when l/h is larger than 2, assuming $l/h = 5$ for further calculation will not only ensure the accuracy of the calculation but also meet the engineering requirements of design simplicity.

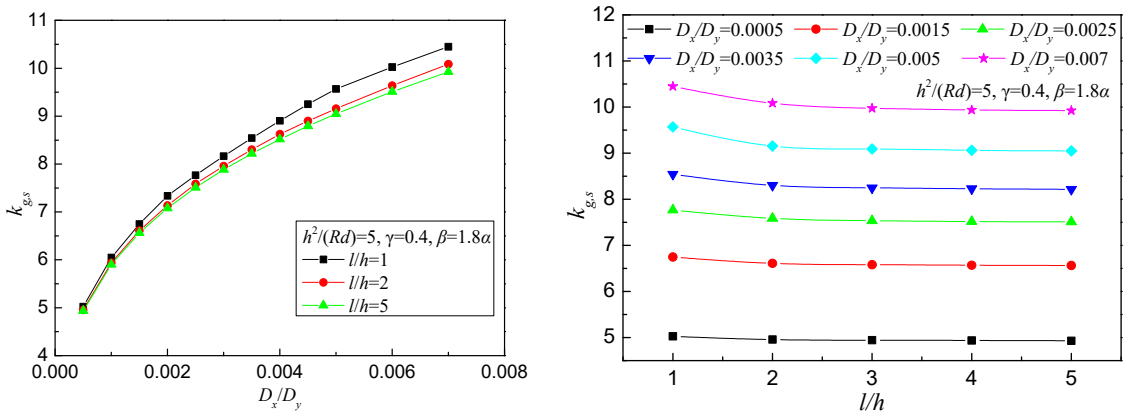

Figure 3. The effect of the rigidity ratio D_x/D_y and the length to height ratio l/h on the global shear buckling coefficient $k_{g,s}$ for the four-edge simple support: (**a**) D_x/D_y on $k_{g,s}$; (**b**) l/h on $k_{g,s}$.

3. Influence of γ on the global shear buckling coefficient k_g

Table 3 lists the values of $k_{g,s}$ for γ equal to 0.38, 0.4, 0.42 and 0.44 respectively when $l/h = 5$, $h^2/(Rd) = 5$ and $\beta = 1.8\alpha$ for the four-edge simple support. The results are practically equal for γ equal to 0.38, 0.4, 0.42 and 0.44. The conclusion remains unchanged when changing the values of l/h, $h^2/(Rd)$, and the boundary conditions. This implies that the modulus ratio γ has little effect on the coefficient k_g for common HCG bridges with CSWs. In what follows, assuming $\gamma = 0.4$ will not only ensure the accuracy of the calculation but also reduce the number of parameters in the parametric study.

Table 3. The effect of γ on the global shear buckling coefficient $k_{g,s}$ when $l/h = 5$, $h^2/(Rd) = 5$ and $\beta = 1.8\alpha$ for the four-edge simple support.

α	γ = 0.38	γ = 0.40	γ = 0.42	γ = 0.44
α = 0.001	5.9044	5.9044	5.9044	5.9044
α = 0.003	7.8894	7.8894	7.8894	7.8894
α = 0.005	9.0580	9.0580	9.0581	9.0581

4. Influence of $h^2/(Rd)$ on the global shear buckling coefficient k_g

Tables 4–6 lists the values of k_g for various values of $h^2/(Rd)$ and D_x/D_y when $l/h = 5$, $\gamma = 0.4$ and $\beta = 1.8\alpha$ for three boundary conditions. Figure 4 shows the effect of $h^2/(Rd)$ and D_x/D_y on the global shear buckling coefficient $k_{g,s}$ for the four-edge simple support. As we can see from Figure 4 and Tables 4–6, the global shear buckling coefficient k_g increases with the increase of the rigidity ratio D_x/D_y and increases slightly with the parameter $h^2/(Rd)$. This implies that the global shear buckling stress of curved bridge webs is slightly higher than that of straight bridge webs. For HCG bridges with $D_x/D_y \leq 0.007$ and $h^2/(Rd) \leq 20$, the global shear buckling stress of curved bridge webs can be calculated conservatively as that of straight bridge webs with a difference less than 2.5%.

Table 4. Global shear buckling coefficient $k_{g,s}$ for various values of $h^2/(Rd)$ and D_x/D_y when l/h = 5, γ = 0.4 and $\beta = 1.8\alpha$ for the four-edge simple support.

$h^2/(Rd)$	D_x/D_y											
	0.0005	**0.001**	**0.0015**	**0.002**	**0.0025**	**0.003**	**0.0035**	**0.004**	**0.0045**	**0.005**	**0.006**	**0.007**
0	4.9321	5.9031	6.5619	7.0786	7.5097	7.8841	8.2169	8.5171	8.7936	9.0482	9.5103	9.9235
5	4.9327	5.9044	6.5642	7.0818	7.5139	7.8894	8.2232	8.5246	8.8024	9.0580	9.5226	9.9386
10	4.9344	5.9085	6.5708	7.0912	7.5266	7.9052	8.2419	8.5468	8.8283	9.0872	9.5592	9.9824
15	4.9373	5.9153	6.5819	7.1068	7.5473	7.9309	8.2726	8.5832	8.8698	9.1348	9.6188	10.0522
20	4.9414	5.9247	6.5973	7.1283	7.5757	7.9658	8.3147	8.6331	8.9261	9.1996	9.6983	10.1463
25	4.9465	5.9368	6.6167	7.1555	7.6110	8.0096	8.3675	8.6951	8.9962	9.2792	9.7946	10.2621
30	4.9527	5.9515	6.6399	7.1881	7.6532	8.0616	8.4300	8.7665	9.0788	9.3706	9.9070	10.3954

Table 5. Global shear buckling coefficient $k_{g,f}$ for various values of $h^2/(Rd)$ and D_x/D_y when l/h = 5, γ = 0.4 and $\beta = 1.8\alpha$ for the four-edge fixed support.

$h^2/(Rd)$	D_x/D_y											
	0.0005	**0.001**	**0.0015**	**0.002**	**0.0025**	**0.003**	**0.0035**	**0.004**	**0.0045**	**0.005**	**0.006**	**0.007**
0	9.3520	11.1647	12.4023	13.3594	14.1630	14.8562	15.4733	16.0290	16.5382	17.0068	17.8556	18.6097
5	9.3521	11.1650	12.4028	13.3602	14.1640	14.8574	15.4748	16.0308	16.5402	17.0091	17.8585	18.6132
10	9.3525	11.1659	12.4044	13.3624	14.1669	14.8611	15.4793	16.0360	16.5463	17.0161	17.8672	18.6237
15	9.3532	11.1675	12.4071	13.3661	14.1718	14.8672	15.4867	16.0447	16.5564	17.0276	17.8817	18.6411
20	9.3541	11.1697	12.4109	13.3713	14.1786	14.8758	15.4971	16.0570	16.5706	17.0437	17.9019	18.6653
25	9.3554	11.1725	12.4157	13.3780	14.1874	14.8868	15.5103	16.0726	16.5887	17.0643	17.9276	18.6963
30	9.3568	11.1760	12.4216	13.3861	14.1990	14.8998	15.5264	16.0917	16.6108	17.0894	17.9587	18.7340

Table 6. Global shear buckling coefficient $k_{g,fs}$ for various values of $h^2/(Rd)$ and D_x/D_y when l/h = 5, γ = 0.4 and $\beta = 1.8\alpha$ for the two edges constrained by flanges fixed and the other two edges simply supported.

$h^2/(Rd)$	D_x/D_y											
	0.0005	**0.001**	**0.0015**	**0.002**	**0.0025**	**0.003**	**0.0035**	**0.004**	**0.0045**	**0.005**	**0.006**	**0.007**
0	9.3514	11.1640	12.4009	13.3583	14.1615	14.8549	15.4721	16.0277	16.5369	17.0056	17.8537	18.6069
5	9.3516	11.1643	12.4014	13.3590	14.1624	14.8561	15.4736	16.0295	16.5389	17.0079	17.8566	18.6104
10	9.3520	11.1653	12.4030	13.3613	14.1654	14.8598	15.4781	16.0347	16.5450	17.0149	17.8655	18.6209
15	9.3526	11.1668	12.4057	13.3650	14.1703	14.8659	15.4855	16.0434	16.5551	17.0265	17.8799	18.6384
20	9.3536	11.1690	12.4095	13.3703	14.1772	14.8744	15.4959	16.0555	16.5693	17.0427	17.9001	18.6628
25	9.3547	11.1718	12.4143	13.3770	14.1860	14.8854	15.5093	16.0710	16.5874	17.0635	17.9261	18.6938
30	9.3562	11.1753	12.4202	13.3852	14.1968	14.8978	15.5255	16.0900	16.6095	17.0887	17.9575	18.7314

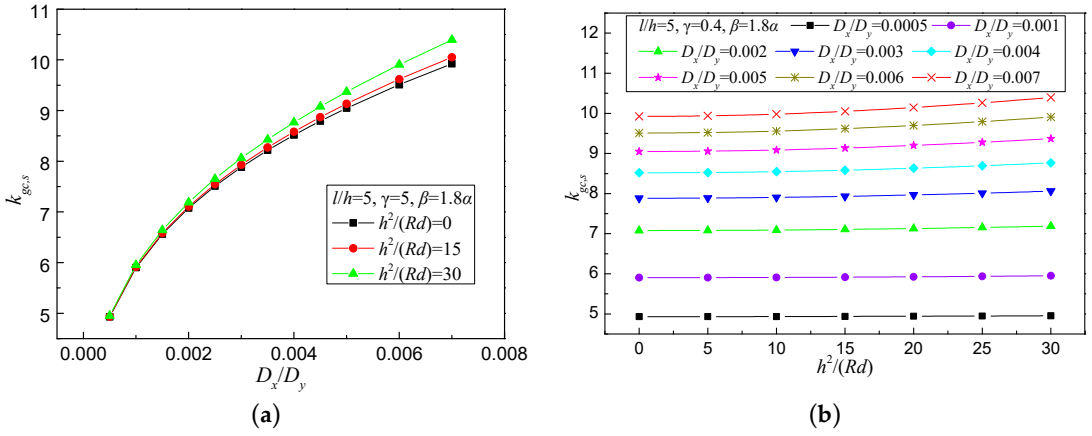

Figure 4. The effect of D_x/D_y and $h^2/(Rd)$ on the global shear buckling coefficient $k_{g,s}$ for the four-edge simple support: (**a**) D_x/D_y on $k_{g,s}$; (**b**) $h^2/(Rd)$ on $k_{g,s}$.

The first row of data for $h^2/(Rd) = 0$ in Tables 4–6 represents the global shear buckling coefficient of CSWs for straight girders. Through fitting of the first-row data in Tables 4–6, for CSWs with $0.0005 \leq \alpha \leq 0.007$, the global shear buckling coefficients $k_{g,s}$, $k_{g,f}$, $k_{g,fs}$ for straight girders can be estimated respectively by Equations (19) and (20).

For a four-edge simple support:

$$k_{g,s} = 36.8\alpha^{0.2648} \tag{19}$$

For a four-edge fixed support, or for two edges constrained by flanges fixed and the other two edges simply supported:

$$k_{g,f} = k_{g,fs} = 67.7\alpha^{0.2608} \tag{20}$$

For trapezoidal CSWs that are commonly used in actual bridges, the rigidity ratio α can be expressed as Equation (21).

$$\alpha = \frac{D_x}{D_y} = \frac{q^2t^2}{2s(3a+c)d^2} \tag{21}$$

It is worth mentioning that the formulas for the global shear buckling stress τ_g^e (Equation (18)) and the global shear buckling coefficient k_g (Equations (19) and (20)) proposed in this paper are slightly different from these proposed by previous researchers [8]. This is due to the fact that while previous researchers derived the formula for the global shear buckling stress τ_g^e the complete CSW was treated as an orthotropic plate with its length much larger than its width, and using a simplified deflection function, which is different from the function used in this paper.

2.3. Elastic Local Shear Buckling Stress of CSWs

Similar to straight girders, the local shear buckling of CSWs for curved girders can also be solved by analyzing a single flat panel constrained by adjacent panels and girder flanges under shear force. For straight and curved girder the same formulas apply for calculating the elastic local shear buckling stress of CSWs which are given by the classical plate buckling theory [3] as Equation (22):

$$\tau_l^e = k_l \frac{\pi^2 E}{12(1-\nu^2)}\left(\frac{t}{p}\right)^2 \tag{22}$$

where k_l is the elastic local shear buckling coefficient of CSWs; p is the maximum sub-panel width (maximum of flat panel width a and inclined panel width c).

The elastic local shear buckling coefficient k_l can be expressed as Equations (23)–(25).

For a four-edge simple support:

$$k_{l,s} = 5.34 + 4(p/h)^2 \tag{23}$$

For a four-edge fixed support:

$$k_{l,f} = 8.98 + 5.6(p/h)^2 \tag{24}$$

For the two edges constrained by flanges fixed and the other two edges simply supported:

$$k_{l,fs} = 5.34 + 2.31(p/h) - 3.44(p/h)^2 + 8.39(p/h)^3 \tag{25}$$

3. Finite Element Analysis

The central angle which depends on the radius of curvature R and girder span L is an important factor for HCGs. A linear FEA is carried out by ANSYS software (ANSYS 12.1, ANSYS Inc., Canonsburg, PA, USA, 2012) [32] to study the influence of R and L on the elastic shear buckling stress of CSWs for HCGs. Three geometries of CSWs that are commonly used in actual bridges are studied here (see Table 7).

Table 7. Studied geometries of CSWs.

Model	a (mm)	b (mm)	c (mm)	d (mm)	θ (°)
CSW900	250	200	250	150	36.9
CSW1200	330	270	336	200	36.5
CSW1600	430	370	430	220	30.6

3.1. Finite Element Modeling

To reduce computational time, only one half of each girder is modeled here. The remainder (the right hand side part) is represented by adequate symmetry boundary conditions. The shell element (shell 181) is used to model the girders with CSWs. The finite element model is shown in Figure 5 and the boundary conditions are given in Table 8, where the edge AB is a roller support and the surface CDEF is a plane of symmetry. All girders are subjected to a concentrated load at the point G located in the plane of symmetry. Junction nodes of flanges and CSWs are constrained in the radial direction (z'-direction), the rotations around the x' axis and y-axis to prevent lateral-torsion buckling.

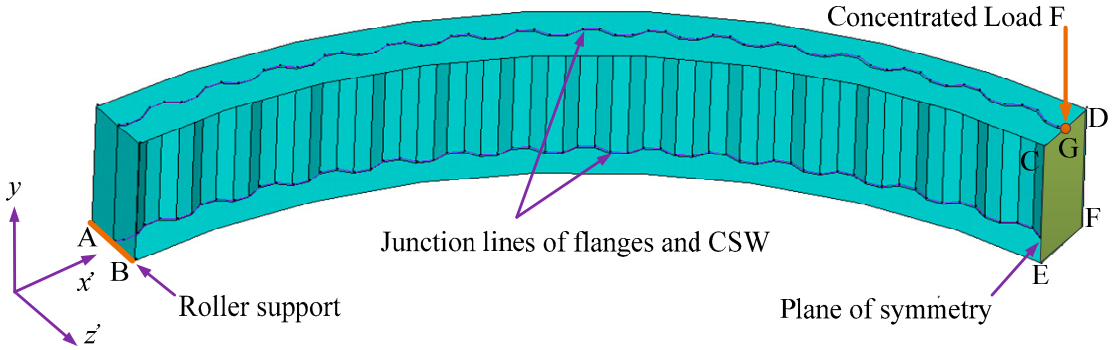

Figure 5. Load and boundary conditions of a curved girder with CSW.

Table 8. Boundary conditions of finite element models.

Boundary	$\delta_{x'}$	δ_y	$\delta_{z'}$	$\theta_{x'}$	θ_y	$\theta_{z'}$
Edge AB	○	●	●	●	●	○
Surface CDEF	●	○	●	●	●	●
Junction nodes	○	○	●	●	●	○

Note: ○: Free; ●: Restrained.

In this study, the radius of curvature R is set at 30 m~150 m, the half span of the girders is set at $5q$~$25q$, the width and the thickness of the flanges are $8d$ and 100 mm respectively. The behavior of the stiffeners is assumed to be rigid. In addition, the number of elements per sub-panel is 6, as suggested by Eldib [2], and the element mesh size is $a/6$. The elastic modulus and poisson's ratio of steel are taken as 210,000 MPa and 0.3 respectively. Figure 6 represents three shear buckling modes of CSWs.

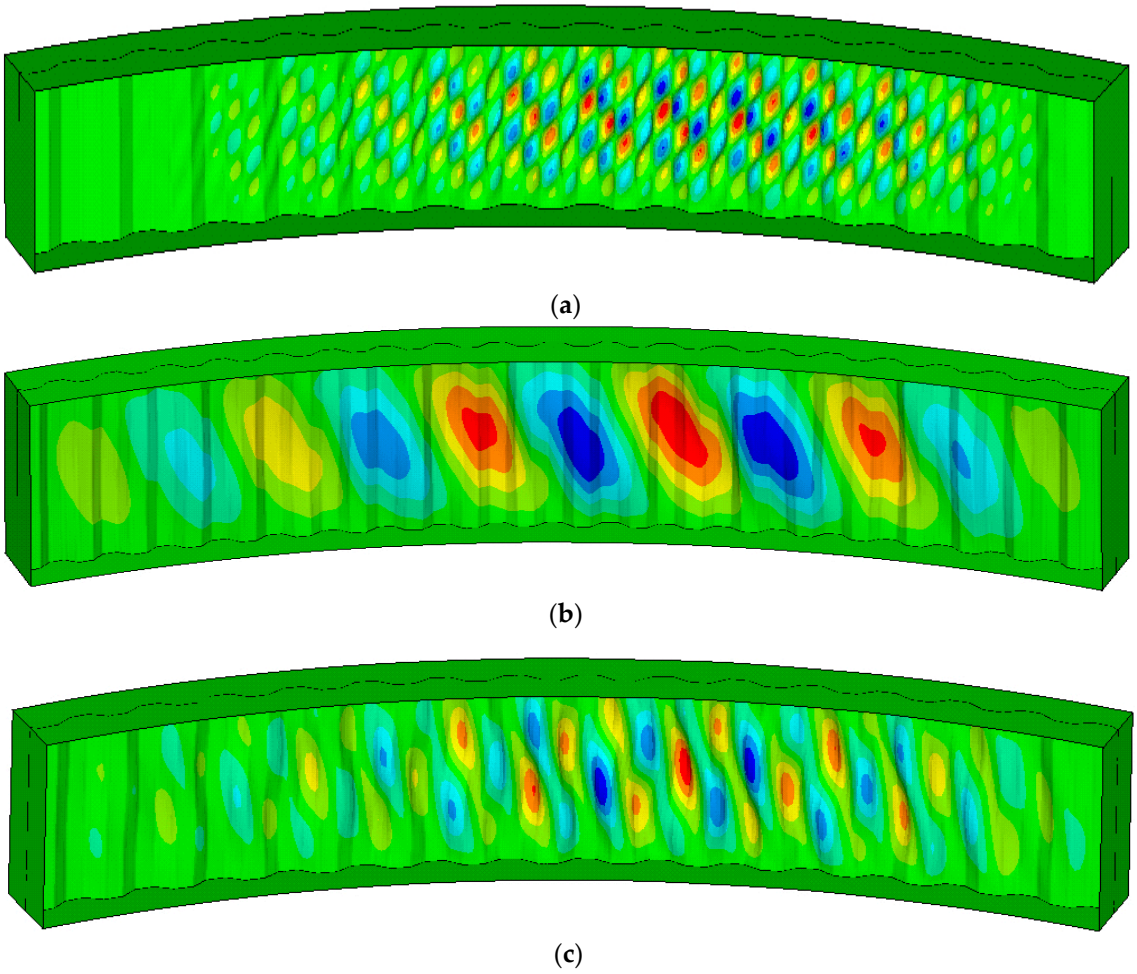

Figure 6. Three shear buckling modes: (**a**) Local shear buckling; (**b**) Global shear buckling; (**c**) Interactive shear buckling.

3.2. Influence of the Radius of Curvature and Girder Span on the Elastic Shear Buckling Stress

Theoretically, the radius of curvature R has only a small influence on the elastic global shear buckling stress and has no influence on the elastic local shear buckling stress. Table 9 shows the elastic shear buckling stress of CSWs for different radii of curvature when $L/2 = 15q$. As we can see from Table 9, the difference of the FEA results between curved girders and straight girders with CSWs is very small which agrees with the theoretical expectations. Table 10 shows the elastic shear buckling stress of CSWs for different spans. It can be seen from Table 10 that the shear buckling stress decreases slightly with the increase of span and the buckling stress shows a converging trend with the increase of the span, which agrees with the theoretical expectations. In Tables 9 and 10, the theoretical stress τ_{cr}^{e} is the minimum of the elastic global and the local shear buckling stress. τ_{FEA}^{e} is the shear buckling stress obtained from FEA. Because the difference of elastic shear buckling stress of CSWs between curved girders and straight girders is very small, the shear buckling stress formulas for straight girders can be applied for curved girders.

Table 9. Elastic shear buckling stress of CSWs for different radii of curvature.

Model	h (mm)	a/h	t (mm)	d/t	R (m)	τ^e_{FEA} (Mpa)	τ^e_{cr} (Mpa)	τ^e_{FEA}/τ^e_{cr}
CSW900	1250	0.2	8	18.8	30	1073.8	1069	1.00
					60	1073.6	1069	1.00
					90	1073.5	1069	1.00
					120	1073.5	1069	1.00
					150	1073.5	1069	1.00
					250	1073.5	1069	1.00
					Straight	1073.5	1069	1.00
	2500	0.1	12	12.5	30	1309.4	1064.4	1.23
					60	1308.5	1064.4	1.23
					90	1308.3	1064.4	1.23
					120	1308.3	1064.4	1.23
					150	1308.3	1064.4	1.23
					250	1308.2	1064.4	1.23
					Straight	1308.2	1064.4	1.23
CSW1200	1650	0.2	8	25	30	655.7	613.5	1.07
					60	653.9	613.5	1.07
					90	654.3	613.5	1.07
					120	654.5	613.5	1.07
					150	654.6	613.5	1.07
					250	654.6	613.5	1.07
					Straight	644.7	613.5	1.05
	3300	0.1	12	16.7	30	933.6	916.2	1.02
					60	931.1	916.2	1.02
					90	931.1	916.2	1.02
					120	931.2	916.2	1.02
					150	931.2	916.2	1.02
					250	931.2	916.2	1.02
					Straight	928.8	916.2	1.01
CSW1600	2150	0.2	10	22	30	596.2	564.6	1.06
					60	588.8	564.6	1.04
					90	595.4	564.6	1.05
					120	595.9	564.6	1.06
					150	596.1	564.6	1.06
					250	596.5	564.6	1.06
					Straight	596.8	564.6	1.06
	4300	0.1	14	15.7	30	712.2	675	1.06
					60	705.5	675	1.05
					90	708.6	675	1.05
					120	708.7	675	1.05
					150	708.7	675	1.05
					250	708.7	675	1.05
					Straight	708.7	675	1.05

Table 10. Elastic shear buckling stress of CSWs for different spans.

Model	R (m)	h (mm)	a/h	t (mm)	d/t	$L/2$	τ^e_{FEA} (Mpa)	τ^e_{cr} (Mpa)	τ^e_{FEA}/τ^e_{cr}
CSW900	30	1250	0.2	8	18.8	5q	1080.1	1069	1.01
						10q	1074.1	1069	1.00
						15q	1073.8	1069	1.00
						20q	1073.8	1069	1.00
						25q	1073.7	1069	1.00
	90	2500	0.1	12	12.5	5q	1334.4	1064.4	1.26
						10q	1312.4	1064.4	1.23
						15q	1308.3	1064.4	1.23
						20q	1306.5	1064.4	1.23
						25q	1304.6	1064.4	1.23
CSW1200	30	1650	0.2	8	25	5q	656.3	613.5	1.07
						10q	655.9	613.5	1.07
						15q	655.7	613.5	1.07
						20q	655.6	613.5	1.07
						25q	655.6	613.5	1.07
	90	3300	0.1	12	16.7	5q	947.1	916.2	1.03
						10q	933.2	916.2	1.02
						15q	931.1	916.2	1.02
						20q	930.1	916.2	1.02
						25q	929.0	916.2	1.01
CSW1600	30	2150	0.2	10	22	5q	597.3	564.6	1.06
						10q	596.5	564.6	1.06
						15q	596.2	564.6	1.06
						20q	596	564.6	1.06
						25q	596	564.6	1.06
	90	4300	0.1	14	15.7	5q	712.2	675	1.06
						10q	710.3	675	1.05
						15q	708.6	675	1.05
						20q	707.5	675	1.05
						25q	705.7	675	1.05

4. Experimental Work

4.1. Geometric Dimensioning of Test Girders

Three single cell box girder test specimens are used for this study. The geometry of the curved box girders is shown in Figure 7. The length is 6.6 m and the radius of curvature is 8 m. The box girders have two or three intermediate steel diaphragms with a thickness of 8 mm. The results of material tests are given in Table 11.

Table 11. Results of the material tests for the steel used for the CSWs.

Specimen	Number of Intermediate Diaphragms	Design Thickness (mm)	Actual Thickness (mm)	Yield Stress (MPa)	Ultimate Stress (MPa)
S1-t1d2	2	1	0.88	187.5	322.4
S2-t2d2	2	2	1.74	263.9	364.9
S3-t2d3	3	2	1.74	263.9	364.9

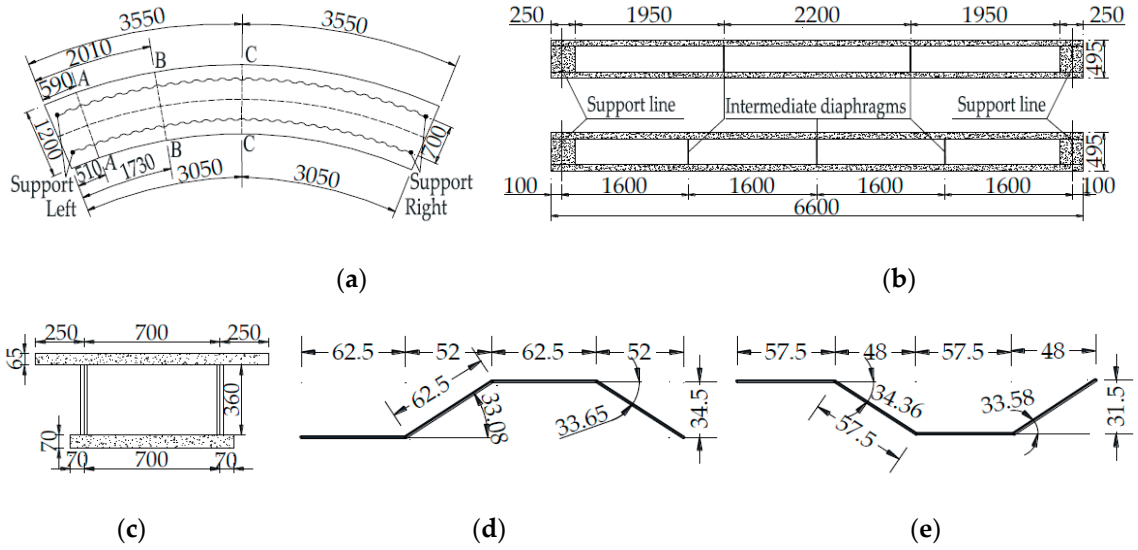

Figure 7. Geometry and dimensions of test girders with CSWs (unit: mm): (**a**) Plan view; (**b**) Elevation view; (**c**) Cross-section; (**d**) Outer CSW; (**e**) Inner CSW. Right: the right-hand side of test girders. Left: the left-hand side of test girders.

4.2. Loading Configurations and Measuring Devices

Figure 8 shows a schematic view of the loading configurations. Both midspan loading and three-point loading are applied in longitudinal direction, one and two-point loading are applied in radial direction. Figure 9 shows the arrangements of strain gauges on S1-t1d1 and S3-t2d3 and those on S2-t2d2 are similar. The size in Figures 8 and 9 express length of arc.

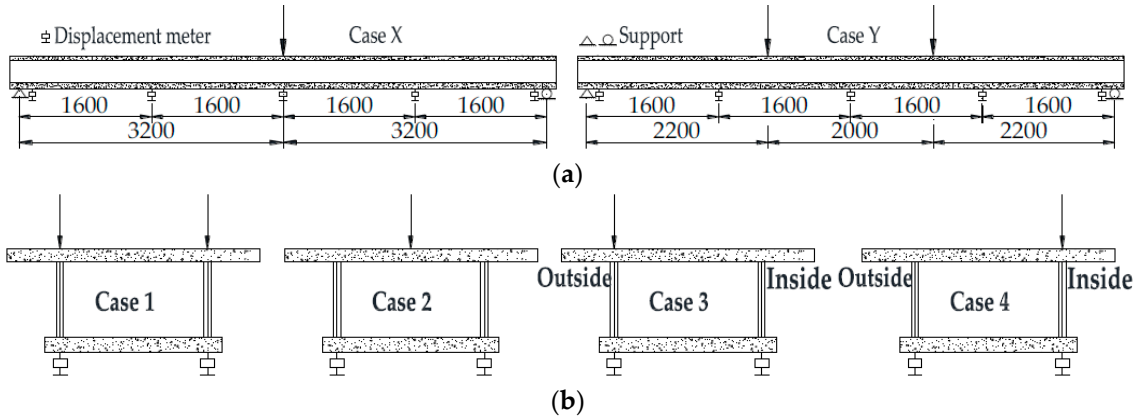

Figure 8. Schematic view of loading configurations: (**a**) Loading points applied in longitudinal direction; (**b**) Loading points applied in radial direction.

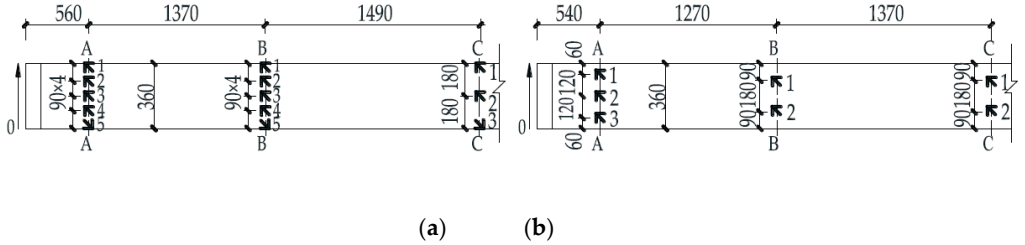

Figure 9. Arrangements of strain gauges on CSWs on S1-t1d2 and S3-t2d3: (**a**) Outer CSW; (**b**) Inner CSW.

Figure 10 shows a photograph of the test setup under the loading configuration of cases X and 2. Other loading configurations are similar. The details of the strain gauge configurations on the CSWs, the load transducers on the supports and the displacement transducers are shown.

(**a**) (**b**) (**c**) (**d**)

Figure 10. Photograph of the test setup: (**a**) Test setup; (**b**) Strain gauge configurations on CSWs; (**c**) Load transducers on supports; (**d**) Displacement transducers.

4.3. Experimental Results

4.3.1. Non-Destructive Test

First, a non-destructive test was carried out. In this test, a midspan loading was applied (see Figure 8 Case X).

As is shown in Figure 9, strain rosette gages were used to measure the strains in three directions. The shear strain γ_w and the principle strain direction angle φ can be calculated by Equations (26) and (27) respectively.

$$\gamma_w = \varepsilon_{0^\circ} + \varepsilon_{90^\circ} - 2\varepsilon_{45^\circ} \tag{26}$$

$$\varphi = \frac{1}{2}\arctan\left(\frac{\gamma_w}{\varepsilon_{90^\circ} - \varepsilon_{0^\circ}}\right) \tag{27}$$

where ε_{0°, ε_{90°, ε_{45° are the strains in horizontal direction, vertical direction, and 45° direction respectively, as shown in Figure 11.

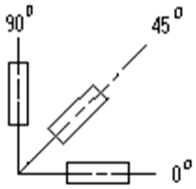

Figure 11. Schematic view of the strain rosette gage.

Figure 12 shows the measured shear strain distributions of the CSWs at sections A and B for specimen S3-t2d3. It can be found that the shear strain distributions are almost uniformly distributed along the direction of the web height. Because the effect of the concrete flanges, the shear strain near flanges shows some deviations. The principal strain direction angles of CSWs are given in Table 12. It can be seen that the direction angles are close to 45°, which indicates that CSWs for HCGs are almost in a pure shear stress state and barely carry axial forces. The results are similar to CSWs of straight girders [22].

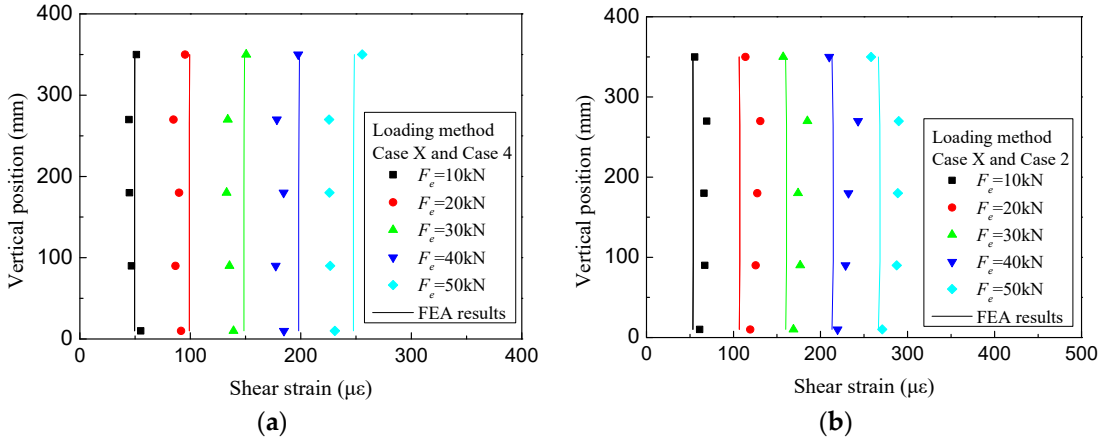

Figure 12. Shear strain distributions of CSWs for specimen S3-t2d3: (**a**) A section; (**b**) B section.

Table 12. Principle strain direction angles of CSWs.

Specimens	Section	Loading Case	Vertical Position (mm)	F_e (kN)				
				10	20	30	40	50
S2-t2d2	B	Case 1	300	41.73°	40.99°	41.29°	41.59°	41.68°
			180	43.17°	44.04°	44.40°	44.59°	44.60°
			60	44.83°	44.55°	44.27°	43.54°	43.31°
S3-t2d3	A	Case 4	350	40.13°	40.77°	40.57°	40.24°	40.49°
			270	42.79°	42.71°	43.44°	43.16°	42.91°
			180	44.24°	44.54°	44.77°	44.77°	44.71°
			90	44.98°	44.86°	44.97°	44.68°	45.00°
			10	44.46°	43.80°	43.93°	43.60°	43.71°

According to structural mechanics, the total shear force of section A and B is 25 kN when applying 50 kN vertical load at midspan. The average shear strain in the same section is used to calculate Q_w, the shear force carried by the CSWs, which can be calculated by Equation (28) due to the uniformly distributed shear strain along the direction of the web height.

$$Q_w = G(\gamma_o + \gamma_i)th \tag{28}$$

where γ_o and γ_i are the average shear strain of the outer web and the inner web respectively. Table 13 shows the ratios of Q_w to the total shear force Q_{total} of specimen S3-t2d3, and the average ratio is 76%.

Table 13. Ratios of Q_w to the total shear force Q_{total} of specimen S3-t2d3.

Specimens	Loading Case	Section	Q_{total} (kN)	Test Results				FEA Results			
				γ_o (10^{-6})	γ_i (10^{-6})	Q_w (kN)	Q_w/Q_{total}	γ_o (10^{-6})	γ_i (10^{-6})	Q_w (kN)	Q_w/Q_{total}
S3-t2d3	Case 2	A	25	327	44	18.8	75.1%	344	34	19.2	76.6%
	Case 2	B		289	98	19.6	78.3%	267	111	19.1	76.6%
	Case 3	A	25	409	−46	18.4	73.5%	442	−62	19.2	76.8%
	Case 3	B		366	14	19.2	76.9%	355	25	19.2	76.7%
	Case 4	A	25	233	128	18.3	73.1%	248	130	19.1	76.5%
	Case 4	B		188	194	19.3	77.3%	181	197	19.1	76.4%

4.3.2. Destructive Tests

(1) Shear Buckling Stress of CSWs

Based on the theoretical formulas (Section 2), the elastic global and local shear buckling stress of CSWs is shown in Table 14. It can be seen from Table 14 that the elastic global and local shear

buckling stresses of CSWs are larger than the shear yield stress of CSWs, that is to say, the occurrence of shear buckling occurs after the yielding of CSWs which meets the general safety criterion of bridge design [33]: yielding before local shear buckling, and local buckling before global shear buckling. In this way the full strength of the girder is mobilized. While local buckling cannot induce girder failure, global shear buckling can. After local buckling the load can still be increased.

Table 14. Shear Buckling Stress of CSWs.

Specimen	CSW	Global Buckling Stress $\tau^e_{g,s}$ (MPa)	Local Buckling Stress $\tau^e_{l,s}$ (MPa)	Uniaxial Yield Stress (MPa)	Shear Yield Stress (MPa)
S1-t1d2	Outer CSW	1542	205.5	187.5	108.2
	Inner CSW	1347.9	241.9	187.5	108.2
S2-t2d2/S3-t2d3	Outer CSW	2212.4	803.3	263.9	152.4
	Inner CSW	1934	945.9	263.9	152.4

(2) Experimental Phenomena and Results

In the destructive tests, a three-point loading was applied (see Figure 8 Case Y and Case 3).

The final deformed shape of the test specimen S1-t1d2 at the end of testing is presented in Figure 13. The final buckling shapes are presented in Figures 14–16. From the experimental phenomena it is clear that local shear buckling occurred first in one of the corrugated panels. Then, with increasing load, the buckling propagated to adjacent panels. In the final state, the interactive shear buckling and the global shear buckling occurred in all specimens. It should be pointed out that the buckling of the CSWs occurred after the yielding of the CSWs which is in good agreement with the theoretical prediction.

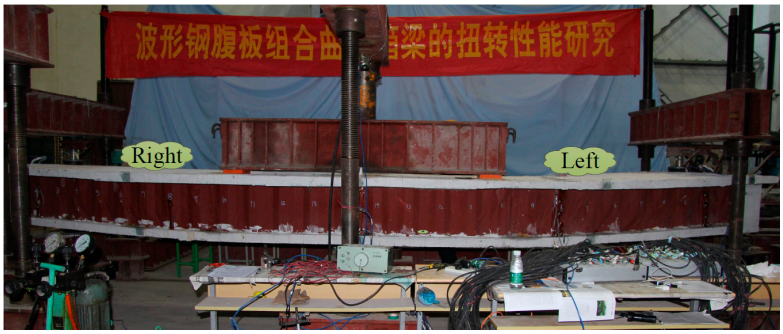

Figure 13. The final deformed shaped of specimen S1-t1d2.

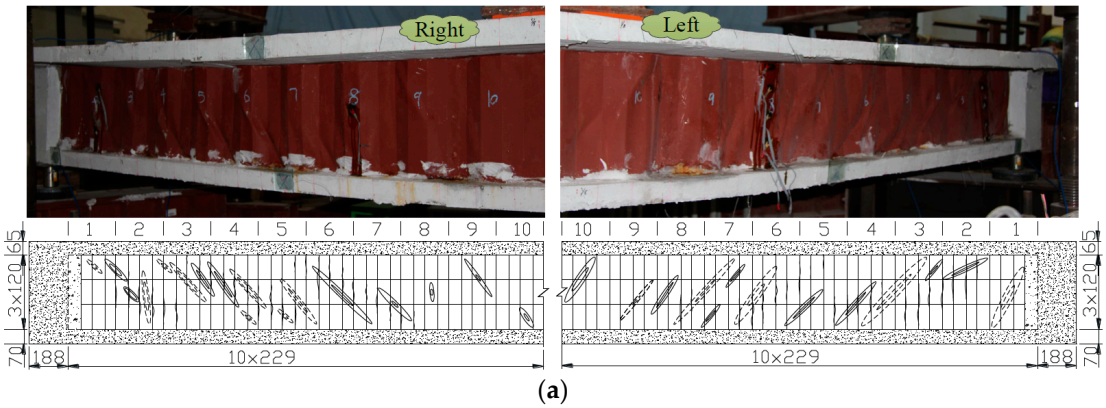

(**a**)

Figure 14. *Cont.*

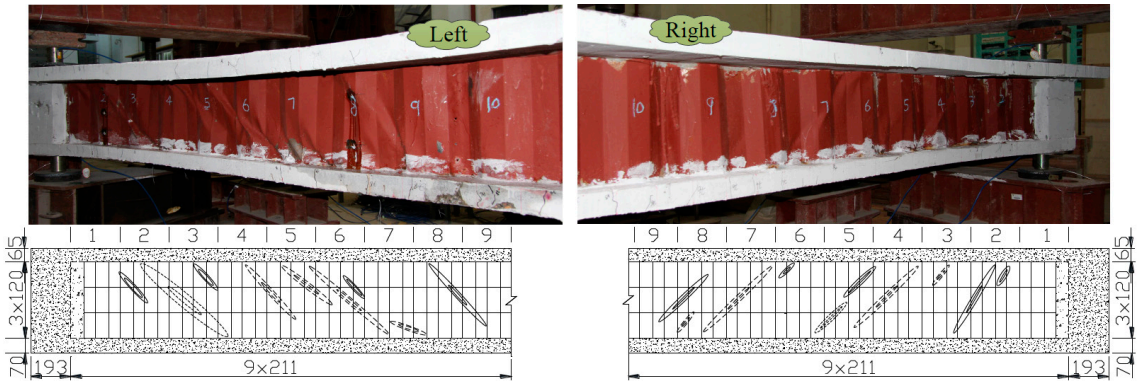

(**b**)

Figure 14. The final buckling shapes of CSWs for specimen S1-t1d2: (**a**) Outer CSW; (**b**) Inner CSW.

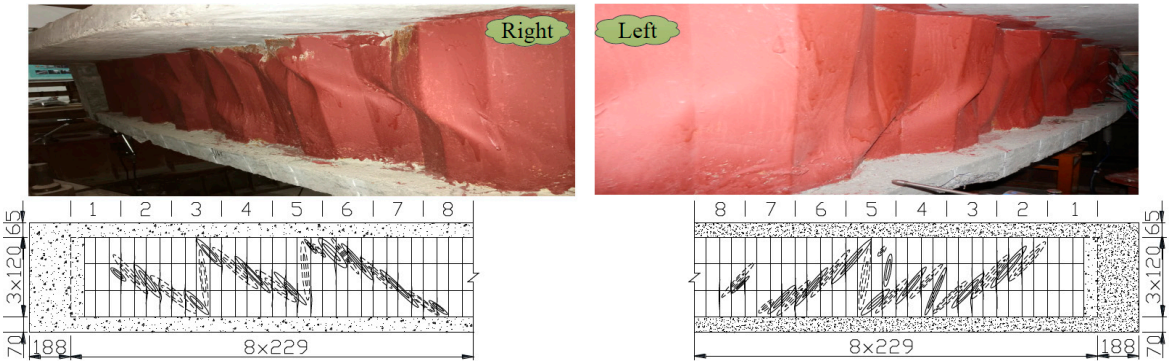

Figure 15. The final buckling shapes of outer CSW for specimen S2-t2d2. Right: the right-hand side of test girders. Left: the left-hand side of test girders.

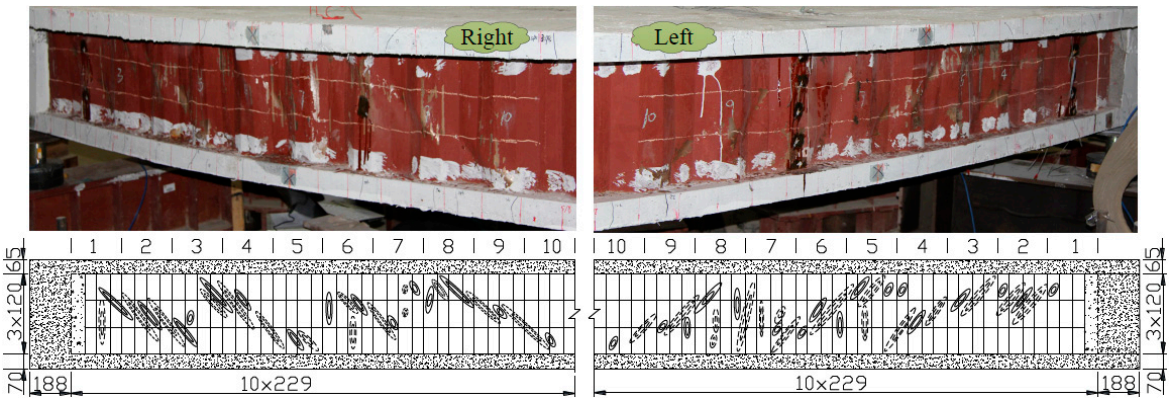

Figure 16. The final buckling shapes of outer CSW for specimen S3-t2d3. Right: the right-hand side of test girders. Left: the left-hand side of test girders.

Figure 17 shows the load-deflection curves of test girders. the curves do not give the displacement state at the stage of critical load due to failure of the displacement meters. The loads at which local buckling occurred are 65.9 kN, 140 kN and 147 kN for S1-t1d2, S2-t2d2, and S3-t2d3 respectively. The critical loads are 94.3 kN, 190 kN, 157.9 kN respectively. This shows that the box girders with CSWs have high post-buckling strength and can continue to resist the load after the occurrence of local shear buckling. Figure 17 also shows the load-deflection curves obtained from FEA results. It can be observed that the FEA results and the test results follow the same trend, and they are in good agreement at the early stage of loading. The agreement is reasonable to good at the later stage of the

loading considering the influence of simultaneous yielding and buckling of CSWs and stiffness loss due to concrete cracking.

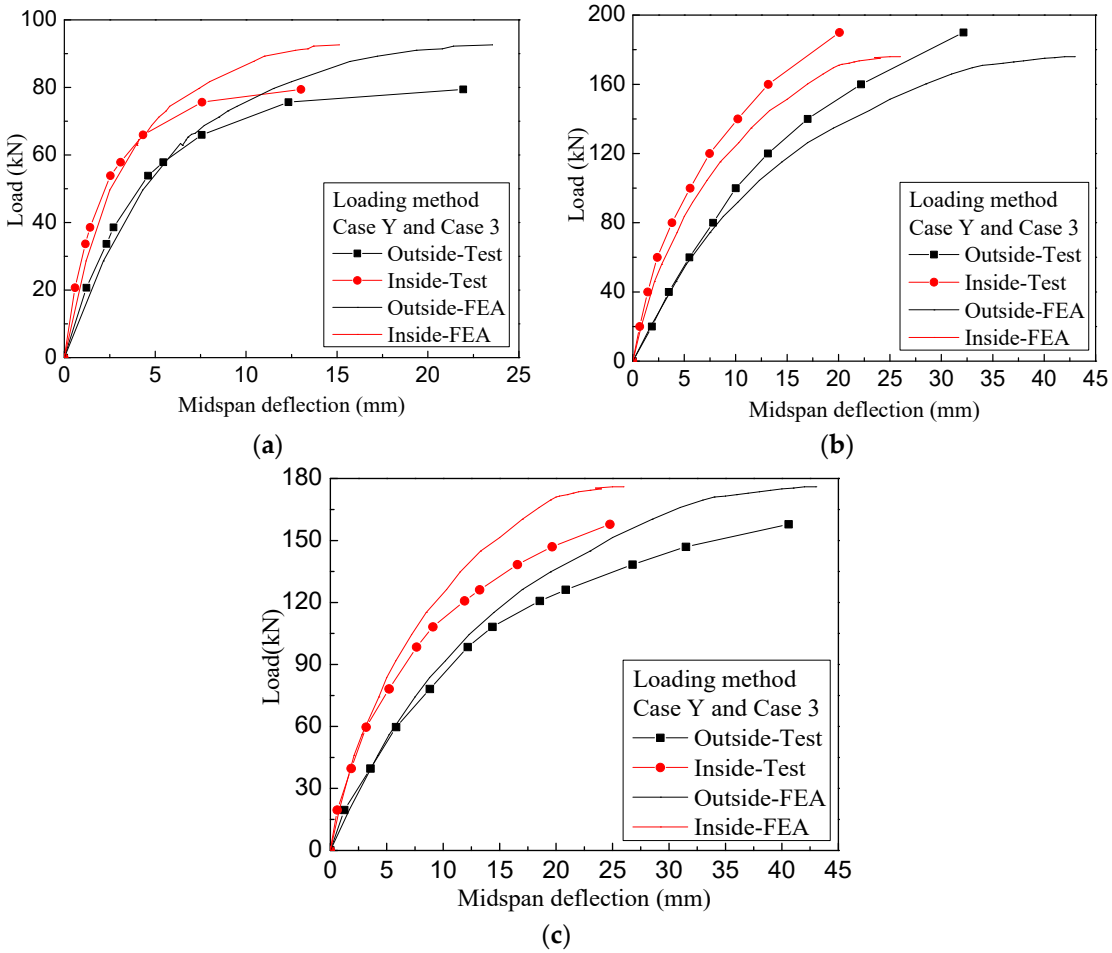

Figure 17. Load-deflection curves of test girders at mid-span section: (**a**) S1-t1d2; (**b**) S2-t2d2; (**c**) S3-t2d3.

5. Conclusions

In this paper, the shear capacity of CSWs for HCGs is theoretically, numerically and experimentally studied, and the following main conclusions can be drawn:

(1) The CSW in HCGs is treated as an orthotropic cylindrical shallow shell, and the analytical formula for the elastic global shear buckling stress is deduced by the Galerkin method. Simplified formulas for the global shear buckling coefficient k_g for a four-edge simple support, for a four-edge fixed support, and for the two edges constrained by flanges fixed and the other two edges simply supported are proposed.

(2) A parametric study based on a linear buckling analysis is performed to analyze the effect of the curvature radius and girder span on the shear buckling stress. Analytical and numerical results show that the difference of shear buckling stress of CSWs between curved girders and straight girders is small, so the shear design formulas for straight girders can be applied for curved girders.

(3) Loading tests were performed on three curved box girders with CSWs. Similar to CSWs in straight girders, the shear strain distributions of CSWs in HCGs are almost uniform along the direction of the web height and the principal strain direction angles are close to 45°. For the three specimens, CSWs carry about 76% of the shear force. In the destructive test, shear buckling after yielding occurred in all specimens which is in good agreement with the theoretical prediction,

which means that the analytical formulas provide good predictions for the shear buckling stress of CSWs in HCGs and can be applied for design purposes.

Author Contributions: S.L. did the derivation of the global shear buckling stress of CSWs for HCGs and performed the finite element analysis and writing. H.D. and S.L. designed and performed the experiment. H.D., L.T. and W.D.C. did the review and editing.

Funding: This research was funded by the National Natural Science Foundation of China, grant number 51378106 and the China Scholarship Council. The financial support is gratefully acknowledged.

Conflicts of Interest: The authors declare no conflict of interest.

References

1. Hamilton, R.W. Behavior of Welded Girders with Corrugated Webs. Ph.D. Thesis, University of Maine, Orono, ME, USA, 1993.
2. Eldib, M.-H. Shear buckling strength and design of curved corrugated steel webs for bridges. *J. Constr. Steel Res.* **2009**, *65*, 2129–2139. [CrossRef]
3. Timoshenko, S.P. *Theory of Elastic Stability*, 2nd ed.; McGraw-Hill Book Company: New York, NY, USA, 1961.
4. Aggarwal, K.; Wu, S.; Papangelis, J. Finite element analysis of local shear buckling in corrugated web beams. *Eng. Struct.* **2018**, *162*, 37–50. [CrossRef]
5. Bergman, S.; Reissner, H. Neuere Probleme aus der Flugzeugstatik–Über die Knickung von Wellblechstreifen bei Schubbeanspruchung. *Z. Flugzeugtechnik Motorluftschiffahrt* **1929**, *20*, 475–481.
6. Hlavacek, V. Shear instability of orthotropic panels. *Acta Technica CSAV* **1968**, *1*, 134–158.
7. Easley, J.T.; McFarland, D.E. Buckling of light-gage corrugated metal shear diaphragms. *J. Struct. Div.* **1969**, *95*, 1497–1516.
8. Easley, J.T. Buckling formulas for corrugated metal shear diaphragms. *J. Struct. Div.* **1975**, *101*, 1403–1417.
9. Peterson, J.P. *Investigation of the Buckling Strength of Corrugated Webs in Shear*; National Aeronautics and Space Administration: New York, NY, USA, 1960.
10. Bergfelt, A.; Edlund, B.; Leiva, L. Trapezoidally corrugated girder webs: Shear buckling, patch loading. *Ing. Arch. Suisses* **1985**, *111*, 22–27.
11. El Metwally, A.; Loov, R.E. Corrugated steel webs for prestressed concrete girders. *Mater. Struct.* **2003**, *36*, 127–134. [CrossRef]
12. Ziemian, R.D. *Guide to Stability Design Criteria for Metal Structures*, 6th ed.; John Wiley & Sons: New York, NY, USA, 2010.
13. Machimdamrong, C.; Watanabe, E.; Utsunomiya, T. Shear buckling of corrugated plates with edges elastically restrained against rotation. *Int. J. Struct. Stab. Dyn.* **2004**, *4*, 89–104. [CrossRef]
14. Yi, J.; Gil, H.; Youm, K.; Lee, H. Interactive shear buckling behavior of trapezoidally corrugated steel webs. *Eng. Struct.* **2008**, *30*, 1659–1666. [CrossRef]
15. El Metwally, A.S. Prestressed Composite Girders with Corrugated Steel Webs. Ph.D. Thesis, University of Calgary, Calgary, AB, Canada, 1998.
16. Abbas, H.H.; Sause, R.; Driver, R.G. Shear strength and stability of high performance steel corrugated web girders. In *SSRC Conference*; German National Library of Science and Technology: Seattle, WA, USA, 2002.
17. Shiratani, H.; Ikeda, H.; Imai, Y.; Kano, K. Flexural and shear behavior of composite bridge girder with corrugated steel webs around middle support. *Doboku Gakkai Ronbunshu* **2003**, *2003*, 49–67. [CrossRef]
18. Sayed-Ahmed, E.Y. Plate girders with corrugated steel webs. *Eng. J.* **2005**, *42*, 1–13.
19. Elgaaly, M.; Hamilton, R.W.; Seshadri, A. Shear strength of beams with corrugated webs. *J. Struct. Eng.* **1996**, *122*, 390–398. [CrossRef]
20. Driver, R.G.; Abbas, H.H.; Sause, R. Shear behavior of corrugated web bridge girders. *J. Struct. Eng.* **2006**, *132*, 195–203. [CrossRef]
21. Moon, J.; Yi, J.; Choi, B.H.; Lee, H.-E. Shear strength and design of trapezoidally corrugated steel webs. *J. Constr. Steel Res.* **2009**, *65*, 1198–1205. [CrossRef]
22. Nie, J.G.; Zhu, L.; Tao, M.X.; Tang, L. Shear strength of trapezoidal corrugated steel webs. *J. Constr. Steel Res.* **2013**, *85*, 105–115. [CrossRef]

23. Hassanein, M.F.; Kharoob, O.F. Shear buckling behavior of tapered bridge girders with steel corrugated webs. *Eng. Struct.* **2014**, *74*, 157–169. [CrossRef]
24. Hassanein, M.F.; Elkawas, A.A.; Hadidy, A.M.E.; Elchalakani, M. Shear analysis and design of high-strength steel corrugated web girders for bridge design. *Eng. Struct.* **2017**, *146*, 18–33. [CrossRef]
25. Leblouba, M.; Junaid, M.T.; Barakat, S.; Altoubat, S.; Maalej, M. Shear buckling and stress distribution in trapezoidal web corrugated steel beams. *Thin-Walled Struct.* **2017**, *113*, 13–26. [CrossRef]
26. Basher, M.; Shanmugam, N.E.; Khalim, A.R. Horizontally curved composite plate girders with trapezoidally corrugated webs. *J. Constr. Steel Res.* **2011**, *67*, 947–956. [CrossRef]
27. Wang, K.; Zhou, M.; Hassanein, M.; Zhong, J.; Ding, H.; An, L. Study on Elastic Global Shear Buckling of Curved Girders with Corrugated Steel Webs: Theoretical Analysis and FE Modelling. *Appl. Sci.* **2018**, *8*, 2457. [CrossRef]
28. McFarland, D.E. An Investigation of the Static Stability of Corrugated Rectangular Plates Loaded in Pure Shear. Ph.D. Thesis, University of Kansas, Lawrence, KS, USA, 1967.
29. Johnson, R.P.; Cafolla, J. Corrugated webs in plate girders for bridges. In *Proceedings of the Institution of Civil Engineers: Structures and Buildings*; Thomas Telford Limited: London, UK, 1997.
30. Luo, Z.D.; Li, S.J. *Anisotropic Material Mechanics*; Shanghai Jiaotong University Press: Shanghai, China, 1994.
31. Batdorf, S.B. *A Simplified Method of Elastic-Stability Analysis for Thin Cylindrical Shells I: Donnell's Equation*; Technical Report Archive Image Library; Langley Aeronautical Lab.: Langley Field, VA, USA, 1947.
32. ANSYS. *ANSYS User's Manual Revision 12.1*; ANSYS, Inc.: Canonsburg, PA, USA, 2012.
33. Zhu, L.; Cai, J.J.; Nie, J.G. Elastic shear buckling strength of trapezoidal corrugated steel webs. *Eng. Mech.* **2013**, *30*, 40–46.